

Original Article

Analytical method for calculating scallop height of helical toroidal cutter in five-axis milling

Hendriko Hendriko*

*Program in Mechatronics Engineering,
Politeknik Caltex Riau, Pekanbaru, Riau, 28265 Indonesia*

Received: 4 January 2018; Revised: 14 July 2018; Accepted: 24 October 2018

Abstract

This paper proposed a method to determine the path scallop of toroidal cutter in five-axis milling during a complex surface machining. A mathematical algorithm was developed by taking into consideration the impact of the helical angle and inclination angle. The applicability of the proposed method was tested using two model parts with diverse surface profiles. The result showed that the method was effectively used to generate the path scallop data. Moreover, the program simulation could also generate the shape of a machined surface. The effect of the helical angle to the scallop height was also tested and the result showed that the helical angle tended to decrease the scallop height. On the other hand, a larger inclination angle produced a larger scallop height. The verification test using Siemens-NX proved that the method was accurate.

Keywords: scallop height, toroidal cutter, grazing toroidal approximation, five-axis milling

1. Introduction

Generally, several variables are used to indicate the quality of a machined surface that include the machining tolerance, scallop height, and surface roughness. In five-axis machining, the scallop height is the most substantial variable in defining the quality of a machined surface. It is affected by: 1) the geometry of cutting tool, 2) the tool orientation, 3) the geometry of part surface, and 4) the length between two successive tool path (step over) (Hendriko, 2017a.) Therefore, the scallop must be controlled so that the expected surface quality can be obtained. The scallop height is difficult to calculate in five-axis milling due to the complicated part surface and tool orientation. Hence, an accurate method to calculate the scallop height is still a challenge in achieving optimal tool path during sculptured surface machining.

In modeling and computing the scallop height, accurate cutter workpiece engagement (CWE) information is very important. Precise geometric information has a direct influence on the precision of scallop height calculations. There

are three common methods used for calculating the CWE: solid model; discrete method; and the analytical approach. Erdim and Sullivan (2012, 2013) used solid modeler based composite adaptive sampled distance fields to calculate the geometric modeling in five-axis milling. Meanwhile Aras and Albedah (2014) proposed closed boundary representation to calculate the surface intersection between the workpiece material and the cutting tool. Other researchers have used discrete methods such as Z-mapping and modified Z-mapping. Kim, Cho, and Chu (2000) used a Z-mapping method to determine the shape of CWE. Then, Wei, Wang, and Cai (2013) proposed a modified Z-mapping algorithm to define CWE in sculptured surfaces. A solid model produces an accurate result, but it also has the drawback of expensive computational cost. Therefore, many researchers have used discrete methods because it is computationally more efficient than the solid model. However, the computational time of the discrete method increases intensely if the precision and accuracy are refined.

Considering these problems, some researchers were attracted to developing an analytical approach to calculate the scallop height and cut geometry in five-axis milling. Compared to discrete approaches and the solid model, the analytical approach was much faster and more accurate. Several studies (Hendriko, 2013, 2015, 2017a, 2017b; Hendriko, Kiswanto, &

*Corresponding author

Email address: hendriko@pcr.ac.id

Duc, 2017; Kiswanto, Hendriko, & Duc, 2014a, 2014b, 2015) developed an analytical method which was called the analytical boundary method (ABS), to calculate the cut geometry of a flat-end cutter and toroidal cutter during sculptured surface machining. From a series of tests, it was found that the proposed method is applicable to calculate CWE accurately. Furthermore, the computational cost of ABS was proven much cheaper than the Z-mapping method.

Many studies have been performed to calculate the scallop height. Several researchers (Bedi, Ismail, & Mahjoob, 1997; Hricora & Napstkova, 2015) investigated the effectiveness of an inclined flat-end cutter in the milling of free-form part surfaces. The results showed that the inclined flat-end cutter generates smaller scallops compared to the ball-end cutter. Other studies (Yigit & Lazoglu, 2015; Wang, Zhang, & Yan, 2016) proposed a method to define the scallop height of a ball-end cutter to achieve optimal step-over. Tunc and Budak (2009) investigated the effect of cutter posture angle to the scallop height in five-axis milling. The results showed that the cutter posture angle significantly influenced the scallop height. In contrast to the cutter posture angle, studies to investigate the effect of helical angle to the scallop height are still quite lacking.

Most studies in the analytical approach addressed the issue of scallop height for toroidal cutter by simply assuming that the curvature was constant and cutter geometry was approximated by two common primitive geometries, either circle or ellipse. Senatore, Segonds, Rubio, and Dessein (2012) calculated the effective radius of a toroidal cutter due to the inclination angle to represent the swept curve. Then, the scallop height with respect to the radius of part surface was determined using an approximated swept curve, and finally, an optimal step-over could be calculated. Others studies (Bedi, Ismail, Mahjoob, & Chen, 1997; Chiou & Lee, 2002; Hricora & Napstkova, 2015; Ozturk *et al.*, 2009; Senatore *et al.*, 2012; Wang *et al.*, 2016; Weinert, Du, Damm, & Stautner, 2004; Yigit & Lazoglu, 2015) used ellipse to represent the inclined flat-end and ball-end mills. Many studies proved that a parametric equation of an ellipse curve could be used precisely to represent the swept curves of an inclined flat-end and ball-end mill. However, this approach is not applicable for a toroidal cutter. A geometrical toroidal cutter is more complex than the flat-end mill and ball-end mill because it is constructed from two faces: cylindrical face and toroidal face. Consequently, calculating the swept curve when the cutter was set with an inclination angle becomes much more complicated. This issue will be proven in the section of implementation and discussion.

In this study, the swept curve was defined by extending the method to identify the lower engagement point (LE-point) which is called the grazing method proposed by Kiswanto *et al.* (2014a). The scallop height was defined as the length between the intersection point of the cutting path to the surface normal. Therefore, the algorithm of the grazing method was then extended so that it could be used to determine the intersection point between two consecutive tool paths. The intersection point of the cutting path was determined using a combination of a coordinate transformation system and algorithm of swept curve. Meanwhile, the surface normal at the instantaneous tool position was determined based on the instantaneous surface shape. In this study, the shape of the part surface at an instantaneous cutter position was defined using three normal vectors mathematically. The ABS proposed by

Kiswanto *et al.* (2015) was used to define the shape of a part surface and calculate the normal distance. In this study, the algorithm to determine the scallop height was developed by taking into consideration the effect of the tool inclination angle and helical angle.

2. Swept Curve Calculation

In this study, the algorithm was derived for a toroidal cutter. Typically, the surface of a toroidal-end cutter is constructed by cylindrical and toroidal faces (Figure 1a). However, despite the construction by two faces, the scallop height is created only by the engagement between the toroidal side and the workpiece material. The shape of the toroidal face in the cutter coordinate frame (CCF) is defined using the following equation,

$$G_T(\varphi; \lambda) \begin{bmatrix} x \\ y \\ z \end{bmatrix} = \begin{bmatrix} (r_m + r \sin \lambda) \sin \varphi \\ (r_m + r \sin \lambda) \cos \varphi \\ r - r \cos \lambda \end{bmatrix} \quad (1)$$

where r is the corner radius of the cutter and r_m is the length between point T to point e (Figure 1a). Meanwhile and denote the toroidal angle and rotational angle, respectively.

In five-axis milling, the cutter can move freely in space because it can be rotated in the x-axis and y-axis directions. A complex part surface can be machined effectively by managing the motion of the cutter with respect to the part surface normal (curvatures).

In this study, three coordinate systems were used to define the location and posture of the cutting tool (Figure 1b). They are global coordinate frame (GCF), which is used as the reference coordinate system, cutter coordinate frame (CCF), and local coordinate frame (LCF). GCF is a permanent frame denoted by the basis vectors x, y, z , while CCF and LCF are represented by u, v, w and X, Y, Z , respectively. The tool inclination angle (α) is normally used in five-axis milling when machining a free-form part surface. The tool rotation angle is formed with respect to CCF and LCF (Figure 1c). For the purpose of coordinate system transformation from CCF to LCF, an appropriate mapping operator $[M]$ is required. The transformation operator involves the tool orientation about the x-axis θ_A , y-axis θ_B , and also the tool displacement at T , which is defined as follows:

$$[M] = \begin{bmatrix} \cos \theta_B & 0 & \sin \theta_B & x_T \\ \sin \theta_A \sin \theta_B & \cos \theta_A & -\sin \theta_A \cos \theta_B & y_T \\ \cos \theta_A \sin \theta_B & \sin \theta_A & \cos \theta_A \cos \theta_B & z_T \\ 0 & 0 & 0 & 1 \end{bmatrix} \quad (2)$$

The cutter coordinate frame with orthogonal basis vector u, v, w , which is located at the bottom center of the cutting tool (point T), was determined by,

$$w = \begin{bmatrix} \cos \alpha & 0 & \sin \alpha \\ 0 & 1 & 0 \\ -\sin \alpha & 0 & \cos \alpha \end{bmatrix} [0 \ 0 \ 1]^T = [\sin \alpha \ 0 \ \cos \alpha]^T \quad (3)$$

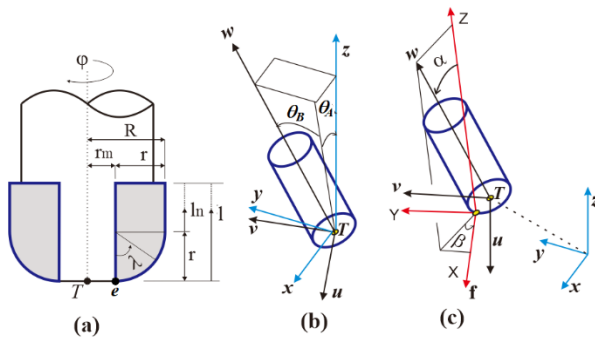


Figure 1. (a) Geometry of the cutting tool, (b) tool orientation relative to GCF, (c) three coordinate systems.

$$v = \frac{w \times V_T}{|w \times V_T|} ; u = v \times w \tag{4}$$

V_T is the linear velocity from cutter location (CL) point to the next and it was calculated as follows:

$$V_T = \frac{CL_{(i+1)} - CL_{(i)}}{f} ; (i = 1,2,3, \dots) \tag{5}$$

There are three points that construct the swept envelope: egress point; grazing point; and ingress point (Chio & Lee, 2002; Weinert *et al.*, 2004). In this study the algorithm to develop the swept curve was derived by improving the method proposed by Kiswanto *et al.* (2014a). The grazing method to determine the lower engagement point in the cut geometry calculation was extended so that it could be used to calculate the swept curve. The swept curve was constructed by a set of swept points at every rotation angle. The swept point can be defined after the toroidal angle (λ) is determined. The swept point is determined using the tangency function:

$$F_{(\vartheta, \varphi, p)} = N_{S_T(\vartheta, \varphi, p)} \cdot V_{S_T(\vartheta, \varphi, p)} = 0 \tag{6}$$

where $N_{S_T(\varphi)}$ is the surface normal of the cutting tool and V_{S_T} is the moving vector of the cutting tool. Then, all of the points at every rotation angle that construct the swept curve are calculated using the same method. The surface normal of an arbitrary point on the cutting tool in CCF is expressed by,

$$N_{S_T} = \frac{\partial S_T / \partial \lambda}{|\partial S_T / \partial \lambda|} \times \frac{\partial S_T / \partial \varphi}{|\partial S_T / \partial \varphi|} = \begin{bmatrix} \sin \lambda \cdot \sin \varphi \\ \sin \lambda \cdot \cos \varphi \\ -\cos \lambda \end{bmatrix} \tag{7}$$

When Equation 7 was mapped to the moving system, it yields,

$$N_{S_T'(\vartheta, \varphi, p)} = \cos(\varphi) \cdot \sin \lambda \cdot v - \cos \lambda \cdot w + \sin \lambda \cdot \sin(\varphi) \cdot u \tag{8}$$

The moving vector of an arbitrary point on the cutting tool was calculated using Equation 9,

$$V_{S_T} = V_T + \overrightarrow{QT} \times \omega \tag{9}$$

where ω and \overrightarrow{QT} denoted the angular velocity and the vector from Q to T , respectively. Since the model was developed by assuming that the tool is static, there was no angular motion ($\omega = 0$). Therefore, the linear velocity is equal to f ($V_T = f$) and the tangency function yields,

$$F_{(\vartheta, \varphi, p)} = \sin \lambda \cdot \sin(\varphi) \cdot (V_T \cdot u) + \sin \lambda \cdot \cos(\varphi) \cdot (V_T \cdot v) + \cos \lambda \cdot (V_T \cdot w) = 0 \tag{10}$$

Since V_T is perpendicular to v , then $V_T \cdot v = 0$. Then, the toroidal angle of swept curve point with respect to the rotation angle is defined as,

$$\lambda_{(\varphi)} = \tan^{-1} \left[\frac{V_T \cdot w}{\sin(\varphi) \cdot (V_T \cdot u)} \right] \tag{11}$$

After $\lambda_{(\varphi)}$ is determined, then, the coordinate of the swept curve point with respect to the rotation angle in the GCF is calculated as follows,

$$I_{(\varphi)}(x_I, y_I, z_I) = [M] S_T(\varphi_I; \lambda_{(\varphi)}) \tag{12}$$

3. Effect of Helical Angle to the Tool Orientation and Swept Surface

The helical angle on the cutting teeth aimed to solve the drawback of straight cutting teeth in which the cutter tooth cuts the material with very strong effort from the beginning. This may cause vibration due to the shock effect and discontinuities of the load that give adverse effects to the quality of the machined surface. Considering this benefit, the helical angle is widely used to overcome this problem. In solid cutting tools, the helical angle (χ) is also called the lag angle. It makes the cutter tooth cut the material gradually. Application of the helical angle changes the geometry of the cut. In this section, the effect of the helical angle on the orientation of the cutting tool and the shape of the swept surface are discussed.

3.1 Identifying the tool orientation angles

In tools without a helical angle, the cutting tool and the cutter tooth have the same orientation. However, when the helical angle is introduced to the cutter tooth, the actual orientation of the cutter tooth is changed. The effect of the helical angle is illustrated in Figure 2a. By assuming a feedrate in the x -direction, then the helical angle changes the orientation of the cutter tooth by rotating the cutter tooth about the y -axis. The orientation of the cutter tooth at every rotation angle is defined by determining the coordinate of two representative points, $s_{\chi}(x_{s_{\chi}}, y_{s_{\chi}}, z_{s_{\chi}})$ and $c(x_c, y_c, z_c)$. The representative points located on the cutter tooth are determined using a parametric equation of cylindrical surface. Point s_{χ} was obtained by rotating point s about the Y -axis by the helical angle. Point s is located arbitrarily on the cutter tooth when $\varphi = 0$. Meanwhile point c is a representative point that was set at the bottom of the cutter tooth. The coordinates of point s and point c in CCF are defined as:

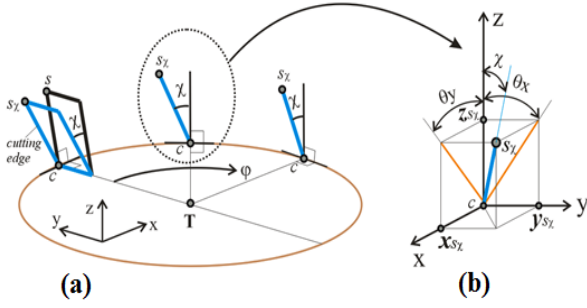


Figure 2. (a) Orientation of the cutter tooth with respect to the rotation angle due to the effect of helical angle. (b) orientation of the cutter tooth.

$$s = (0, r_m, r + 5) \text{ and } c = (0, r_m, r) \quad (13)$$

Then point s_χ and point c as a function of rotation angle are calculated by transforming point s and point c about the Y -axis by the helical angle and about the Z -axis by the rotation angle. They are calculated as follows:

$$s_\chi \begin{bmatrix} x_{s_\chi} \\ y_{s_\chi} \\ z_{s_\chi} \end{bmatrix} = Rot(Z, \varphi) \times Rot(Y, \chi) \times [s] \quad (14)$$

$$s_\chi \begin{bmatrix} x_{s_\chi} \\ y_{s_\chi} \\ z_{s_\chi} \end{bmatrix} = \begin{bmatrix} \cos \varphi & -\sin \varphi & 0 \\ \sin \varphi & \cos \varphi & 0 \\ 0 & 0 & 1 \end{bmatrix} \times \begin{bmatrix} \cos \chi & 0 & \sin \chi \\ 0 & 1 & 0 \\ \sin \chi & 0 & \cos \chi \end{bmatrix} \times \begin{bmatrix} x_s \\ y_s \\ z_s \end{bmatrix} \quad (15)$$

$$c \begin{bmatrix} x_c \\ y_c \\ z_c \end{bmatrix} = Rot(Z, \varphi) \times [c] = \begin{bmatrix} \cos \varphi & -\sin \varphi & 0 \\ \sin \varphi & \cos \varphi & 0 \\ 0 & 0 & 1 \end{bmatrix} \begin{bmatrix} x_c \\ y_c \\ z_c \end{bmatrix} \quad (16)$$

The orientation of the cutting tool relative to GCF due to the helical angle is determined by calculating the orientation of the cutter tooth relative to the X -axis and Y -axis (Figure 2b). They are calculated as follows:

$$\theta_{A_x} = \theta_x = \tan^{-1} \left(\frac{y_{s_\chi} - y_c}{z_{s_\chi}} \right) \quad (17)$$

$$\theta_y = \tan^{-1} \left(\frac{x_{s_\chi} - x_c}{z_{s_\chi}} \right) \quad (18)$$

$$\theta_{B_x} = \tan^{-1} \left(\frac{(x_{s_\chi} - x_c) \cos \theta_{A_x}}{z_{s_\chi}} \right) \quad (19)$$

$$= \tan^{-1} \left(\tan \theta_y \cos \theta_{A_x} \right)$$

In five-axis milling, the orientation of the cutter can be set to any direction due to the complexity of the part surface. Two additional degrees of freedom allow the tool in five-axis milling to be rotated about the X -axis and Y -axis. The rotation

angles about the X -axis and Y -axis are denoted by θ_A and θ_B , respectively. These angles are used to set up the tool to the desired orientation. However, when a helical angle was applied to the cutter tooth, the orientation of the cutter tooth changed significantly. Therefore, the actual orientation of the cutter tooth with respect to GCF needs to be determined. Once again, it was determined using point s_χ and point c . In this case, point s_χ and point c are not only rotated by χ , but also rotated by θ_A and θ_B . Then, Equations 14 and 15 change to become:

$$s_\chi (x_{s_\chi}, y_{s_\chi}, z_{s_\chi}) = Rot(X, \theta_A) \times Rot(Y, \theta_B) \times Rot(Z, \varphi) \times Rot(Y, \chi). [s] \quad (20)$$

$$c(x_c, y_c, z_c) = Rot(X, \theta_A) \times Rot(Y, \theta_B) \times Rot(Z, \varphi). [c] \quad (21)$$

Once s_χ and c were determined, then the actual cutter tooth orientations (θ_{A_x} , θ_{B_x}) can be defined using Equations 17 through 19. Finally the transformation operator to define the orientation and position of the cutter tooth when the tool has a helical angle with respect to θ_{A_x} and θ_{B_x} was defined as follows:

$$[M]_h = Rot(X, \theta_{A_x}) \times Rot(Y, \theta_{B_x})$$

$$[M]_h = \begin{bmatrix} \cos \theta_{B_x} & 0 & \sin \theta_{B_x} \\ \sin \theta_{A_x} \sin \theta_{B_x} & \cos \theta_{A_x} & -\sin \theta_{A_x} \cos \theta_{B_x} \\ -\cos \theta_{A_x} \sin \theta_{B_x} & \sin \theta_{A_x} & \cos \theta_{A_x} \cos \theta_{B_x} \end{bmatrix} \quad (22)$$

3.2 The swept curve of helical cutting tool

For a non-solid cutting tool, the helical angle not only changes the orientation of the cutter tooth, but also changes the shape of the swept surface. The helical angle causes the radius of the swept surface at the upper side to be different than the one at the lower side (Figure 3a). The radius of the swept surface equal to R is only at the lowest side. Meanwhile at the upper side, the radius enlarges gradually as the tool axial height (l) increases. Therefore, the radius of the swept surface as a function of axial height, $R_{\chi(l)}$, was defined by referring to Figure 3b as follows:

$$\psi = \tan^{-1} \left(((r - r \cos \lambda) \sin \chi) / (r_m + r \sin \lambda) \right) \quad (23)$$

$$R_{\chi}(\lambda) = (r_m + r \sin \lambda) / \cos \psi \quad (24)$$

$$G_{T_\chi}(\varphi; \lambda) = \begin{bmatrix} R_{\chi} \sin \varphi \\ R_{\chi} \cos \varphi \\ (r - r \cos \lambda) \cos \chi \end{bmatrix} \quad (25)$$

where $0 < \lambda < 90$ and ψ is the lag angle (Figure 2a). The lag angle is the rotation angle of s_χ relative to the rotation angle of s .

4. Path Intersection Point

The scallop height (h_s) was defined as the normal length between the path intersection point (PIP) to the part surface normal (p_n). The PIP is an intersection point between

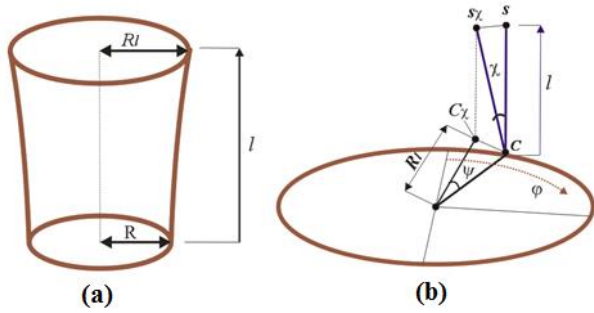


Figure 3. (a) Shape of swept surface using helical cutting tooth, (b) lag angle.

the swept curve of the current cutting path and of the adjacent cutting path. The equations to obtain the path intersection point were derived by referring to Figure 4. Since the tool orientation was set without a tilt angle, the angle of the cutter contact point (τ), which is the deviation angle of the cutting tool relative to the surface normal, was similar. It also put the PIP in the middle of point CC_1 and CC_2 . The distance of the intersection point to the cutter contact (CC) point, which is represented by m , and the angle of the CC point relative to the part surface are calculated by,

$$m = |CC_1 - CC_2|/2 \quad (26)$$

$$\tau = \sin^{-1}(m/R_1) \quad (27)$$

where $R_1 = \sqrt{R_x^2 + R_y^2}$. R_x and R_y are the radii of the part surface at the instantaneous tool position calculated using the method of Kiswanto *et al.* (2015). In this method, the part surface normal (\mathbf{p}_n) was defined mathematically using a set of discrete normal vectors. At any instantaneous tool position, the part surface is defined as a combination of a convex, concave, flat, or sloped surface.

Regarding the cutter orientation by the angle of CC point (τ), the coordinate of the swept point in CCF was mapped to LCF. The mapping coordinate system is performed using the following equation:

$$I_C \begin{bmatrix} x_{I_C} \\ y_{I_C} \\ z_{I_C} \end{bmatrix} = \begin{bmatrix} 1 & 0 & 0 \\ 0 & \cos \tau & -\sin \tau \\ 0 & -\sin \tau & \cos \tau \end{bmatrix} \times G_{T_x}(\varphi_{I_C}; \lambda_{I_C}) \quad (28)$$

The coordinate of $I_C (x_{I_C}, y_{I_C}, z_{I_C})$ can be determined after the toroidal angle of PIP (λ_{I_C}) is defined. With respect to CCF, $y_{I_C} = m$. Since y_{I_C} was identified, λ_{I_C} is defined by extracting Equation 28 only for y_{I_C} as follows:

$$y_{I_C} = \left((r_m + r \sin \lambda_{I_C}) \cos \psi_T \cos \varphi_{I_C} \right) \cos \tau - \left((r - r \cos \lambda_{I_C}) \cos \chi \right) \sin \tau \quad (29)$$

Three unknown variables exist in Equation 29, $\cos \psi_T$, λ_{I_C} , and $\cos \varphi_{I_C}$. Therefore, $\cos \psi_T$ and $\cos \varphi_{I_C}$ need to

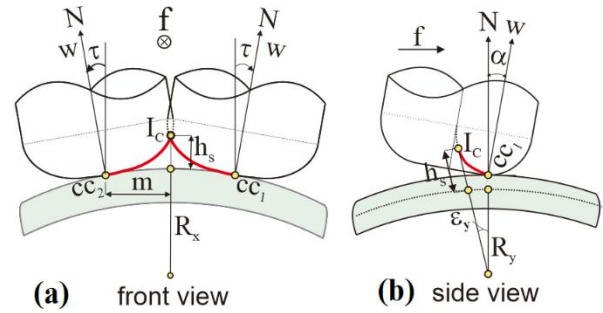


Figure 4. Intersection point of adjacent tool path: (a) front view, (b) side view.

be converted so that only λ_{I_C} is the remaining unknown. By rearranging Equation 11, then $\cos \varphi_{I_C}$ is expressed by:

$$\cos \varphi_{I_C} = \left[\frac{\sqrt{((V_T \cdot u) \sin \lambda_{I_C})^2 - ((V_T \cdot w) \cos \lambda_{I_C})^2}}{(V_T \cdot u) \sin \lambda_{I_C}} \right] \quad (30)$$

Meanwhile $\cos \psi_T$ is obtained by rearranging Equation 23 to become:

$$\cos \psi_T = \left[\frac{(r_m + r \sin \lambda_{I_C})}{\sqrt{((r - r \cos \lambda_{I_C}) \sin \chi)^2 + (r_m + r \sin \lambda_{I_C})^2}} \right] \quad (31)$$

After converting $\cos(\varphi_{I_C})$ and $\cos \psi_T$ in Equation 29 by $\cos(\varphi_{I_C})$ in Equation 30 and $\cos \psi_T$ in Equation 31, finally, Equation 29 yields a polynomial equation as follows:

$$(a^2)t^8 + (2ab)t^7 + (2ac + b^2 + f^2)t^6 + (2ad + 2bc)t^5 + (2ae + 2bd + c^2 - f^2 + 2fg)t^4 + (2be + 2cd)t^3 + (2ce + d^2 - 2fg + g^2)t^2 + (2de)t + (e^2 - g^2) \quad (32)$$

where,

$$t = \sin \lambda_{I_C}$$

$$a = [(r^2 \cos^2 \tau)(1 - \sin^2 \chi) + r^2(V_T \cdot u)^2 \sin^2 \tau]$$

$$b = [2r_m r \cos^2 \tau]$$

$$c = \left[\begin{array}{l} (r^2 \cos^2 \tau \sin^2 \chi)(2 - (V_T \cdot w)^2) \\ + (\cos^2 \tau)(r_m^2 - r^2(V_T \cdot w)^2) \\ + ((V_T \cdot u)^2) \\ (-s^2 - 2r s \cos \chi \sin \tau - 2r^2 \cos^2 \chi \sin^2 \tau) \end{array} \right] \quad (33)$$

$$d = [-2r_m r (V_T \cdot w)^2 \cos^2 \tau]$$

$$e = [(V_T \cdot w)^2 \cos^2 \tau] (-2r^2 \sin^2 \chi - r_m^2)$$

$$f = \left[\begin{array}{l} (2r(V_T \cdot u)^2 \cos \chi \sin \tau)(-s - r \cos \chi \sin \tau) \\ + (2r^2 \cos^2 \tau \sin^2 \chi) \end{array} \right]$$

$$g = [-2r^2(V_T \cdot w)^2 \cos^2 \tau \sin^2 \chi]$$

Eight possibilities of t can be generated by Equation 32. Among them, however, only one t was appropriate to define λ_{Ic} for defining the PIP. The appropriate one was chosen using the following rules: a) t must be within 0 and 1 and b) λ_{Ic} that gives $y_{Ic} = s$ will be selected. Once λ_{Ic} is obtained, the rotation angle can be determined using Equation 11. The coordinate of PIP, $I_C(x_{Ic}, y_{Ic}, z_{Ic})$, is defined by,

$$I_C(x_{Ic}, y_{Ic}, z_{Ic}) = [M]_h G_{T_x}(\varphi_{Ic}; \lambda_{Ic}) \tag{34}$$

Meanwhile $\cos \psi_T$ is obtained by rearranging Equation 23 to become:

$$h_s = \sqrt{I_c^2 - p_n^2} \tag{35}$$

5. Implementation and Discussion

All equations derived in this study were used to develop a program simulation using MATLAB. The proposed method in this study was called Grazing Toroidal Approximation (GTA). In this section, the applicability of the proposed method to calculate the scallop height was checked.

In the first test, the drawback of previous analytical studies in using ellipse to represent the swept curve was proven. The second test demonstrated the ability of GTA to calculate

the scallop height. Finally, the accuracy of the proposed method was examined by comparing the scallop height obtained using Siemens-NX.

5.1 Grazing toroidal approximation versus ellipse curve approximation

The proposed method was tested to check the applicability in generating the swept curve on the toroidal cutter as well as the influence of inclination angle to the shape of swept curve. In this test, a toroidal cutter with a diameter of 20 mm and a minor radius of 5 mm was used as the cutting tool. The swept curve on the toroidal cutter is illustrated in Figure 5a. Figure 5b shows a sample of the swept curve on the cutter when the inclination angle exists, which was then projected into 2D. The projected swept curves for various inclination angle are depicted in Figure 5c. It can be seen that the shape of the swept curve was much influenced by the inclination angle. When the inclination angle was set to negative, the swept curve was located at the back of cutter tooth (Figure 5c). The toroidal angle of the swept curve tends to increase as the inclination angle increased. Figure 5b compares the shape of the projected curve and ellipse curve for various inclination angles. As mentioned in the Introduction, one of the drawbacks of the existing analytical method in scallop calculation is usually researchers use a parametric equation of ellipse to represent the swept curve. It can be seen that the shape of the projected curve was very dynamic and it cannot be approximated by an ellipse when the inclination is small. From a series of tests, it was found that the projected curve coincides precisely with the ellipse curve when the tool used a large inclination angle ($>40^\circ$) (Figure 5d). However, in real machining a large inclination angle is avoided. Hence, it was proved that the ellipse curve approximation method for a toroidal cutter tends to produce an error.

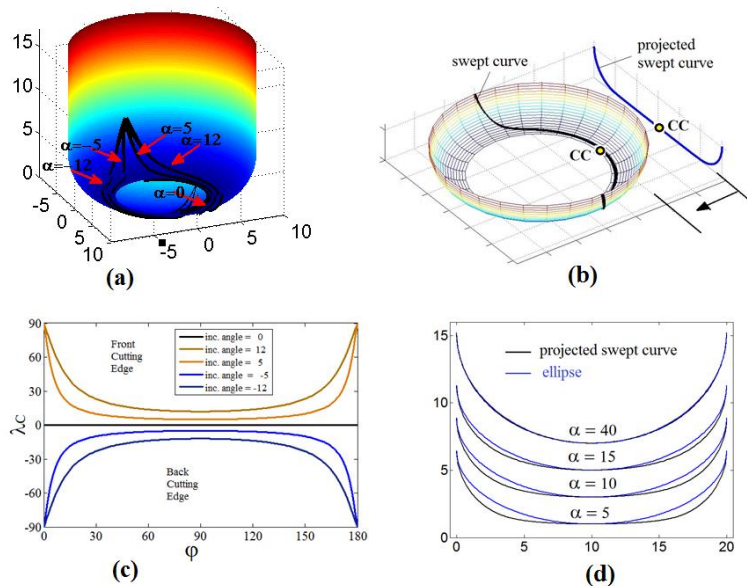


Figure 5. (a) Swept curve on toroidal cutter, (b) projected swept curve, (c) the shape of projected swept curve for various inclination angle, (d) comparison between projected swept curve and ellipse curve.

5.2 Implementation of the grazing toroidal approximation

In this section, the applicability of the proposed method was verified for a model test (Figure 6a). For simplifying the verification process, the test was performed using a large step-over so that a large scallop was obtained. In this test, a 15 mm step-over was selected. The machining conditions set in the test were feedrate 0.3 mm/tooth and spindle speed 5000 rpm. A two-tooth toroidal cutter with a helical angle of 10, a diameter of 20 mm, and a minor radius of 5 mm were used as the cutting tool. Using the GTA, the shape of the machined surface could be generated (Figure 6b). From Figure 6a and Figure 6b, the shape of the machined surface generated using Siemens-NX resembled the shape of the machined surface generated using the program simulation. The shape of the scallop can also be seen in more detail in Figure 6b. Moreover, the coordinate of the intersection point could be determined and hence the scallop height could be calculated. The scallop height generated using the GTA is presented in Figure 6c. The orientation of the cutting tool and the shape of the part surface were continuously changed during the machining process which caused the scallop height to fluctuate during the machining process.

To ensure the ability of the method to calculate the scallop height, another test using a model was performed (Figure 7a). The milling conditions set in this test were feedrate 0.3 mm/tooth and spindle speed 7000 rpm. The tool used in the test was a two teeth toroidal cutter with a diameter of 25 mm and a minor radius of 5 mm. The inclination angle was set to decrease gradually during the ramp-up machining process and then increase gradually during ramp-down milling. Using the same part model and cutting tool, the machining tests were performed using two different step-over values, 20 mm and 10 mm. The shape of the machined surface generated using Siemens-NX is shown in Figure 7a. Using the program simulation, the shape of the machined surface could be generated (Figure 7b). The details of the scallop including the

intersection point and the method to measure the scallop height are depicted in Figure 7c. The shape of the cut produced by program simulation that is shown in Figure 7b resembled the shape of the machined surface generated using Siemens-NX (Figure 7a). The scallop height for each CC point was calculated using the program simulation and the results for a two step-over are presented in Figure 7d. From this figure it can be concluded that increasing the step-over value increases the scallop height.

5.3 Verification of the grazing toroidal approximation

The proposed method was verified using the commercial software Siemens-NX. The shape of the part surface after machining using Siemens-NX is presented in Figure-6a. Although the shapes of machined surfaces were similar, the accuracy of the developed method had to be verified. The verification was carried out by a comparison

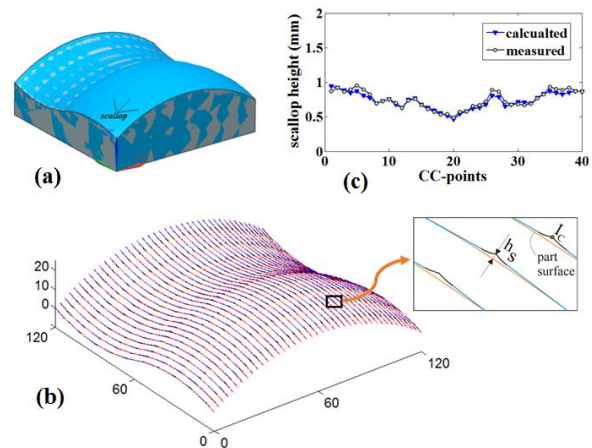


Figure 6. (a) Model test, (b) machined surface generated using proposed method, (c) calculated and measured scallop height.

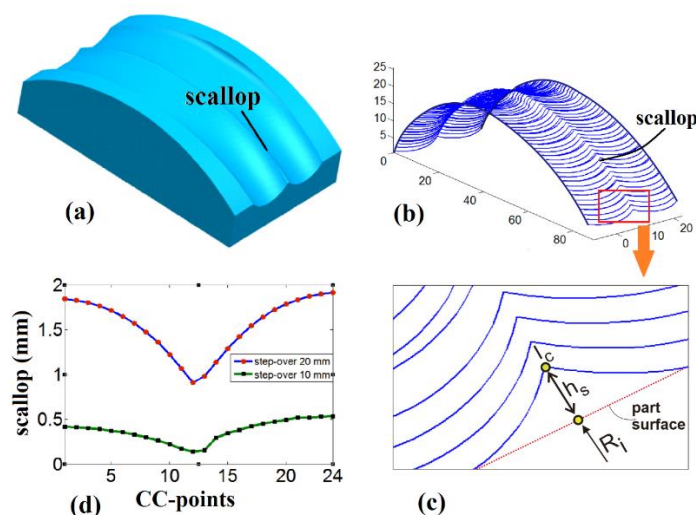


Figure 7. (a) Model test generated using Siemens-NX, (b) machined surface generated using proposed method, (c) details of the scallop, (d) the scallop height for two step-over values.

between the scallop height generated by the proposed method and the measurements using Siemens-NX. The method to measure the cutter workpiece engagement in Siemens-NX was explained by Kiswanto *et al.* (2014a) and Kiswanto *et al.*, (2015).

Based on the tool path data (G-Code), the geometry of the swept volume can be constructed using Siemens-NX. The machined surface was then obtained by extracting the workpiece material using the swept volume model. After the machined surface was obtained, the coordinate of a point on the machined surface could be checked. Finally, the scallop height could be determined by calculating the distance between an intersection point on the machined surface to the designed surface. The scallop heights of all CC points for one tool pass were generated and the results are presented in Figure 6c. The graph shows that the deviation of the verification data is relatively small. In general, the errors were less than 7%.

5.4 Test on the effect of helical angle and inclination angle to scallop height

The ability of the proposed method to check the effect of helical angle to the scallop was also performed. For the verification purpose, a part model was examined (Figure 8a). The machining conditions set in the test were feedrate 0.3 mm/tooth, step-over value 10.49 mm, and spindle speed 5000 rpm. The toroidal cutter with a diameter of 20 mm and a corner radius of 5 mm was used as the cutting tool. The inclination angle was set to decrease gradually during the ramp-up machining process. In this test, the scallop height produced by the toroidal tool was tested using five different helical angles: 0, 10, 20, 30, and 40.

The shape of the machined surface for one tool pass is presented in Figure 8b. The magnitudes of the scallop height for all variables used in the test are presented in Figure 8c. This figure demonstrates that the scallop height decreased gradually as the inclination angle decreased during the ramp-up process. The same result was also demonstrated by a previous test (Figure 7d). The scallop height decreased gradually as the inclination angle decreased during the ramp-up process (from CC point 0 to CC point 12). Then, the scallop increased gradually as the inclination angle increased during the ramp-down process (from CC point 13 to 24). The scallop height during the ramp-down process showed a larger trend than the ramp-up process.

The helical angle significantly affected the scallop height (Figure 8c). At the same machining condition, the helical angle tended to decrease the scallop height. This effect occurred due to the change of the swept surface caused by the existence of the helical angle as discussed in previous section (Figure 3). Increasing the cutter diameter at the upper side caused the intersection between the cutting tool in two subsequent tool passes to produce a smaller uncut material.

6. Conclusions

In this study, the Grazing Analytical Approximation method was extended by taking into consideration the effect of a helical angle. This method was developed to generate a scallop height for a toroidal cutter during five-axis milling. Several important conclusions can be drawn. First, the test proved that the extended GTA is applicable to define the scallop height of a helical toroidal cutter in five-axis milling process. Second, a verification test was performed to compare the scallop heights obtained using the GTA with those measured using Siemens-NX which proved that the GTA is accurate. Third, the test also showed that increasing the helical angle decreases the scallop height. On the other hand, decreasing the inclination angle decreases the scallop height.

Acknowledgements

This research was funded by the Ministry of Research, Technology and Higher Education through the fundamental research grant scheme.

References

- Aras, E., & Albedah, A. (2014). Extracting cutter/workpiece engagements in five-axis milling using solid modeler. *International Journal of Advanced Manufacturing Technology*, 73(9), 1351–1362.
- Bedi, S., Ismail, F., Mahjoob, M. J., & Chen, Y. (1997). Toroidal versus ball nose and flat bottom end mills. *International Journal of Advanced Manufacturing Technology*, 13(5), 326-332.
- Chiou, C. J., & Lee, Y. S. (2002). Swept surface determination for five-axis numerical control machining. *International Journal of Advanced Manufacturing Technology*, 42, 1497-1507.
- Erdim, H., & Sullivan, A. (2012). High accuracy computation of geometric properties of cutter workpiece intersection using distance fields for NC milling. *Procedia CIRP*, 4, 84–89.
- Erdim, H., & Sullivan, A. (2013). Cutter workpiece engagement calculations for five-axis milling using composite adaptively sampled distance fields. *Procedia CIRP* 8, 438–443.
- Hendriko, Duc, E., & Kiswanto, G. (2013). Analytical cut geometry prediction for free form surface during semi-finish milling. In *Proceeding of ASME 2013 International Manufacturing Science and Engineering Conference Collocated with the 41st North American Manufacturing Research Conference* (pp. V001T01A024-V001T01A024). New York, NY: American Society of Mechanical Engineers.

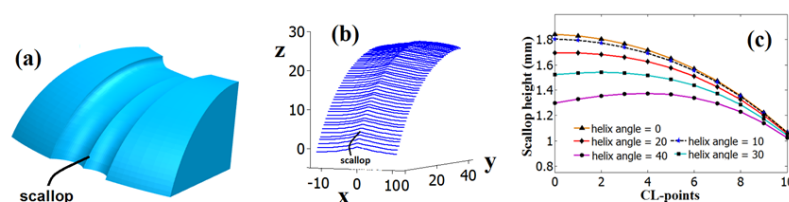


Figure 8. (a) Model test, (b) shape of scallop, (c) scallop height for various helical angles.

- Hendriko, H. (2015). Mathematical model for chip geometry calculation in five-axis milling. *Jurnal Teknologi*, 77(23).
- Hendriko, H. (2017a). Analytical boundary method for obtaining feed scallop of toroidal cutter in multi-axis milling. *Key Engineering Materials*, 728, 48-53.
- Hendriko, H. (2017b). Mathematical model for calculating scallop height of toroidal cutter in five-axis milling. *ARPJ Journal of Engineering and Applied Sciences*, 12(19), 5642-5646.
- Hendriko, H., Kiswanto, G., Istiyanto, J., & Duc, E. (2017). Implementation of analytical boundary simulation method for cutting force prediction model in five-axis milling. *Machining Science and Technology*, 1-17.
- Hricova, J., & Naprstkova, N. (2015). Surface roughness optimization in milling aluminium alloy by using the Taguchis design of experiment. *Manufacturing Technology*, 15(4), 553-509.
- Kim, G. M., Cho, P. J., Chu, C. N. (2000). Cutting force prediction of sculptured surface ball-end milling using Z-map. *International Journal of Machine Tools and Manufacture*, 40(2), 277-291.
- Kiswanto, G., Hendriko, H., & Duc, E. (2014a). An analytical method for obtaining cutter workpiece engagement during a semi-finish in five-axis milling. *Computer-Aided Design*, 55, 81-93.
- Kiswanto, G., Hendriko, H., & Duc, E. (2014b). Analytical method for obtaining cut geometry of helical toroidal cutter during semi-finish in 5-axis milling. *Applied Mechanics and Materials*, 541, 780-784.
- Kiswanto, G., Hendriko, H., & Duc, E. (2015). A hybrid analytical and discrete based methodology for determining cutter workpiece engagement in five axis milling. *International Journal of Advanced Manufacturing Technology*, 80(9), 2083-2096
- Ozturk, E., Tunc, L. T., & Budak, E. (2009). Investigation of lead and tilt angle effects in 5-axis ball-end milling processes. *International Journal of Machine Tools and Manufacture*, 49(14), 1053-1062.
- Senatore, J., Segonds, S., Rubio, W., & Dessein, G. (2012). Correlation between machining direction, cutter geometry and step-over distance in 3-axis milling: Application to milling by zones. *Computer-Aided Design*, 44(12), 1151-1160.
- Wei, Z. C., Wang, M. J., Cai, Y. J., & Wang, S. F. (2013). Prediction of cutting force in ball-end milling of sculptured surface using improved Zmap. *International Journal of Advanced Manufacturing Technology*, 68, 1167-1177.
- Wang, P., Zhang, S., & Yan, Z. G. (2017). Study on surface defects in five-axis ball-end milling of tool steel. *The International Journal of Advanced Manufacturing Technology*, 89(1-4), 599-609.
- Weinert, K., Du, S., Damm, P., & Stautner, M. (2004). Swept volume generation for the simulation of machining processes. *International Journal of Machine Tools and Manufacture*, 44, 617-628.
- Yigit, I. E., & Lazoglu, I. (2015). Analysis of tool orientation for 5-axis ball-end milling of flexible parts. *CIRP Annals-Manufacturing Technology*, 64(1), 97-100.